The role of geometry on controlled cavity collapse and top jet drop

Nilofar Taraki[1], A. Said Ismail[1*]

[1] School of Engineering and Materials Science, Queen Mary University of London, London E1 4NS, United Kingdom

Corresponding author: a.ismail@qmul.ac.uk

Abstract

The contents of this work explore the influence of three geometric parameters on controlled cavity collapse at liquid interface and the subsequent ejected drop; the parameters are the angle of the ejecting nozzle plate (θ), the height (H) and the radius (R) of the vessel used to enclose the liquid within. The conducted computational modelling shows that changing the angle of the nozzle plate from a flat surface to inclined surface in one direction causes the droplet diameter to decrease, whereas an inclination in the opposite direction results in larger droplets. Moreover, changing the height of the fluid vessel does not actually influence the drop size and its velocity as long as the vessel height is much larger than the nozzle radius (R_0). Below the limit $H=5R_0$, the droplet size starts to decrease and its velocity to increase by decreasing the vessel height. Finally, the droplet size decreases by increasing the radius of the fluid vessel even when $R>>R_0$. This is attributed to the change in the displaced liquid volume and subsequently the cavity volume at the tip of the nozzle when the vessel radius is changed.

1. Introduction

Controlled droplet generation is a crucial process to the development of various scientific technologies. An example is presented within the agricultural industry as it heavily relies on the efficient application of pesticides and plant protection products, which is directly influenced by the resultant droplet size and velocity distribution[1]. If the droplet is too small, there is a chance that high winds will remove the product once it has been applied to the plant leaf. On the other hand, if the droplet is too large, excess product will be applied to the leaf resulting in reduced efficiency and overall profits. Therefore, analysis into the characteristics that influence the droplet size would be beneficial in the progression of the agricultural industry, as a major concern for crop producers is the death of plants due to harmful organisms. Additionally, advancements of inkjet technology are vital to ensure that accurate levels of various substances are applied correctly to their corresponding substrates; the uses of such technology range from the delivery of drugs into the body[2] to conventional printing[3]. Controlling the droplet size to minimize the volume of substance delivered is a key factor in applications such as pixels printing and DNA sequencing analysis[4]. Minimizing the drop size is usually achieved by reducing the nozzle size. However, this reduction in size increases the chances of nozzle's blockage and breaking.

The phenomenon explored within the confines of this paper, to generate controlled droplets, is known as Cavity Collapse ejection, a process that can be seen in nature, when a bubble bursts on free liquid surface. The process starts when the bubble film, separating the cavity from the atmosphere, breaks up into tiny droplets[5]. This film rupture also creates capillary waves converging to the axis and resulting in an emerging jet from the cavity[6]. Comparable drops/drop to the jet are/is then separated from the jet depending on different parameters. The bubble bursting process happens every day and has a great influence on how some diseases are transmitted[7] and on our environmental system[8]. For example, in ocean-atmosphere exchange,$10^{12} – 10^{14}$ kg per year of sea salt emission, which causes cloud nucleation, is due to the spray produced out of bubble bursting[9]. The size of the droplets produced influence both the composition and transport of the sea spray aerosols[10,11].

The cavity collapse jets are finite; thus, it breaks through an end pinching mechanism. This mechanism adopts mainly a competition between the capillary force on the jet tip and the inertia[12]. The drop end pinching and separation from the jet happens when the inertia overcome the surface tension. Many studies have been conducted to explore the physical parameters affecting the collapse process. Krishnan et al. found that the cavity size and liquid viscosity influence the collapse time and subsequently the jetting velocity[13]; the precursor capillary waves are damped by decreasing the cavity size or increasing viscosity, which leads to an increase in jet velocity. Because the viscosity reduces the momentum of the capillary wave, this consequently yields a smaller top jet droplet[14]. It was found that the jetting process happens when the cavity is large enough, or the viscosity is sufficiently low to have an energetic wave for the collapse. This occurs at Ohnesorge number $Oh<0.043$[15].

One way to control the process is by using a controlled cavity collapse device[16]. This device usually consists of a liquid filled reservoir with a flat plate nozzle fixed on one end, and a piston or a piezoelectric plate on the other end. The idea is to create a pull-push-pull pressure pulse inside the reservoir to create and collapse the cavity at the nozzle opening leading to a production of droplets much smaller in size than the nozzle. The controlled cavity collapse, unlike the bubble bursting, allows for other parameters, such as meniscus shape, piston velocity amplitude and pulse width, to have a significant impact on droplet production[17]. Scaling laws

that include the liquid properties, the driving waveform pulse and the nozzle size have been developed to characterize the size and velocity of the jetted droplet from this device[17]. However, the effect of other geometrical parameters aside from the nozzle diameter have not been explored yet.

This paper aims to investigate, using numerical simulation, the effect of varying the nozzle plate angle, vessel height and vessel radius on the cavity collapse process to optimise the system and better control the generated droplet size and velocity. This will further improve current technology in a variety of fields that rely on higher resolution droplets and controlled droplet production.

2. Methodology

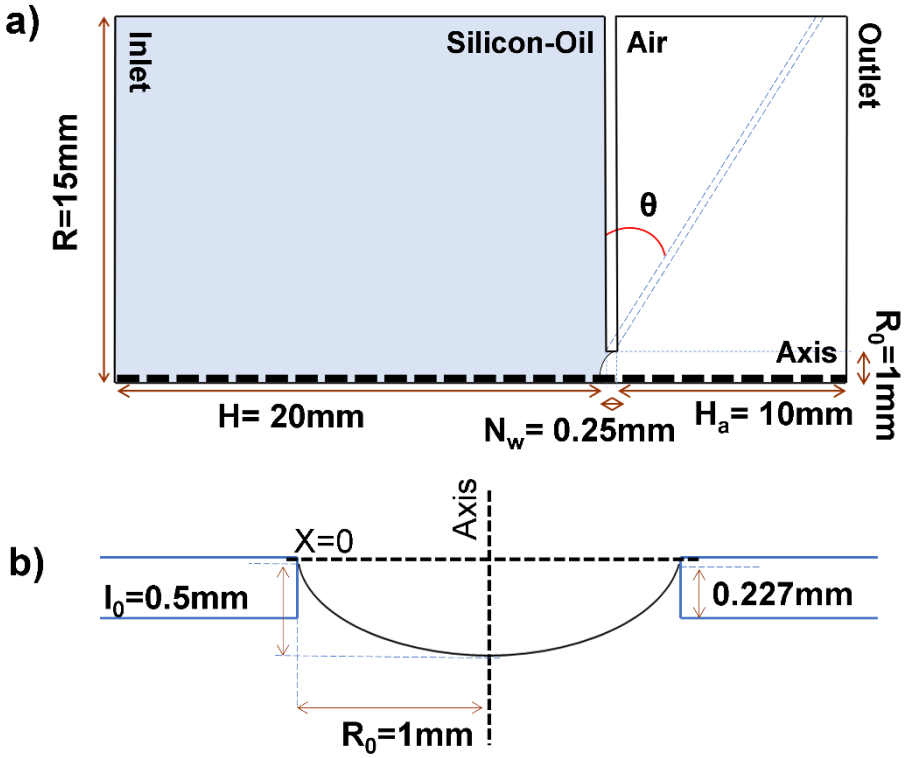

FIG. 1. Sketch of (a) axisymmetric section of the cavity collapse device with full dimensions of the apparatus, and (b) liquid meniscus at the nozzle opening.

A computational model, that was previously developed and validated by the authors[17], was used to obtain the results in this work. The model has an axisymmetric computational domain with the geometrical parameters illustrated in Fig. 1(a). This domain represents an enclosed reservoir containing the liquid (in sky blue colour), air region (in white), and nozzle plate in between. The multiphase flow was simulated in Fluent software using the Volume of Fluid (VoF) solver which is a simplified version of the conventional Eulerian approach for continuous problems. The liquid properties are the density ρ_l, viscosity μ_l and surface tension between both phases σ, whereas the corresponding air properties of density and viscosity are denoted as ρ_g and μ_g. The fluids are assumed to be incompressible and immiscible thus the Navier-Stokes equations that govern the fluids are

$$\nabla \cdot \mathbf{v} = 0, \tag{1}$$

$$\rho\left(\frac{\partial \mathbf{v}}{\partial t} + \mathbf{v} \cdot \nabla \mathbf{v}\right) = -\nabla \mathrm{p} + \nabla \cdot [\mu(\nabla \mathbf{v} + \nabla \mathbf{v}^{\mathrm{T}})] + \mathbf{F_s}, \tag{2}$$

where $\mathbf{v}$, p, and $\mathbf{F_s}$ represent the velocity field, the pressure, and the surface tension term.

The volume fraction of liquid α_l, is used to track the interface position within the computational domain dictated by the transport equation,

$$\frac{\partial}{\partial t}(\alpha_l) + \nabla \cdot (\alpha_l \mathbf{v}) = 0. \tag{3}$$

The volume fraction is then used to determine the values of the both spatially varying density $\rho(\mathbf{x},t)$ and viscosity $\mu(\mathbf{x},\mathrm{t})$ per cell throughout the domain,

$$\rho = \alpha_l \rho_l + \rho_g(1 - \alpha_l), \tag{4}$$

$$\mu = \alpha_l \mu_l + \mu_g(1 - \alpha_l), \tag{5}$$

where $\mathbf{x}$ and t represent the space throughout the domain and the time.

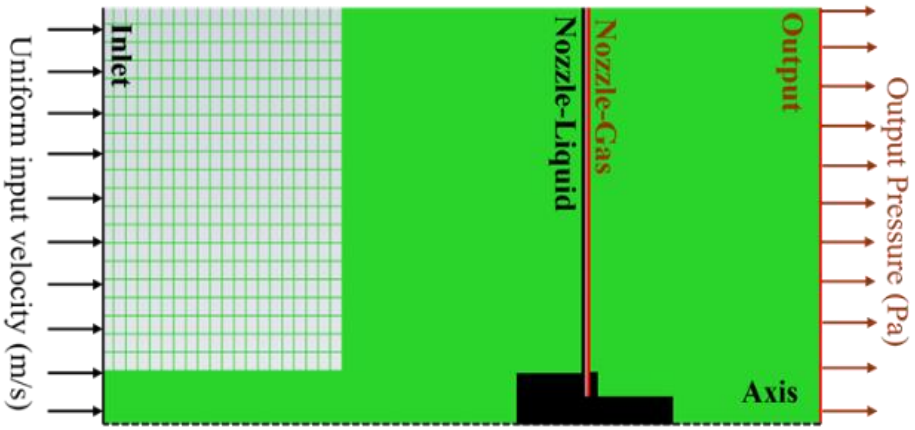

FIG. 2. Computational domain at 0°, showing the mesh and the boundary conditions. The region in black indicates the refined region close to the nozzle opening.

In this work we investigated the effects of changing the nozzle plate angle (θ), height (H) and radius (R) of the fluid vessel. Therefore, other parameters such as nozzle radius (R_0), nozzle plate thickness (N_w) and height of the air space domain (H_a) were kept fixed at 1 mm, 0.25 mm, and 10 mm respectively, for all results produced. The initial shape of the meniscus at the tip of the nozzle is known to influence the cavity collapse process[17]. Therefore, to ensure the reliability of our results, the meniscus shape was kept the same for all the simulations, with the dimensions illustrated in Fig. 1(b).

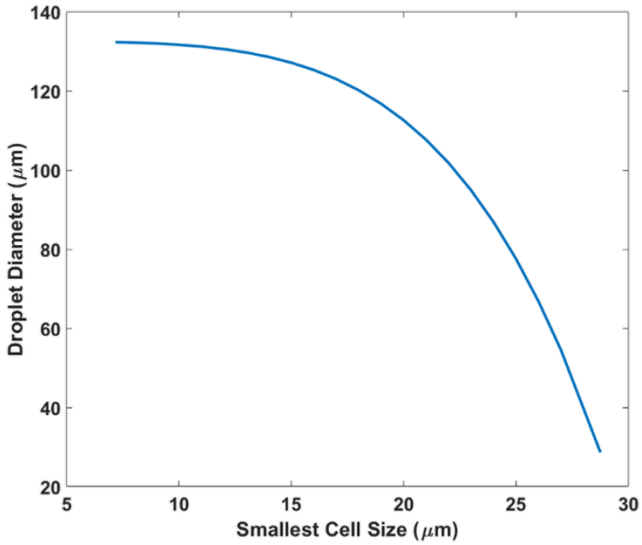

FIG. 3. Mesh sensitivity testing.

The computational domain consisted of around 147627 cells with minimum cells' size of 0.0001 mm^2 close to the nozzle as indicated within the black regions in Fig. 2. We implemented higher levels of mesh refinement closer to the nozzle area, to increase the accuracy and prevent numerical diffusion from occurring at the liquid interface. A mesh refinement analysis was conducted to ensure that the discrepancy between droplet diameter values was not notably large at this level of refinement, thus ensuring the values had reached a point of convergence (see Fig. 3). Upon changing the nozzle plate angle, the geometry was altered to maintain a consistent cell size; therefore, the output wall and the nozzle plate were set to be parallel as shown in Fig. 4. The angle of the nozzle plate was set at 0º for all the simulations conducted to study the change of the vessel radius and height, likewise, the vessel radius and height were kept at 15 mm and 20 mm respectively for the study of the angle variation. We examined the variation of the air region length of the domain (labelled as Ha) and verified that it has no effect on the droplet size nor its speed.

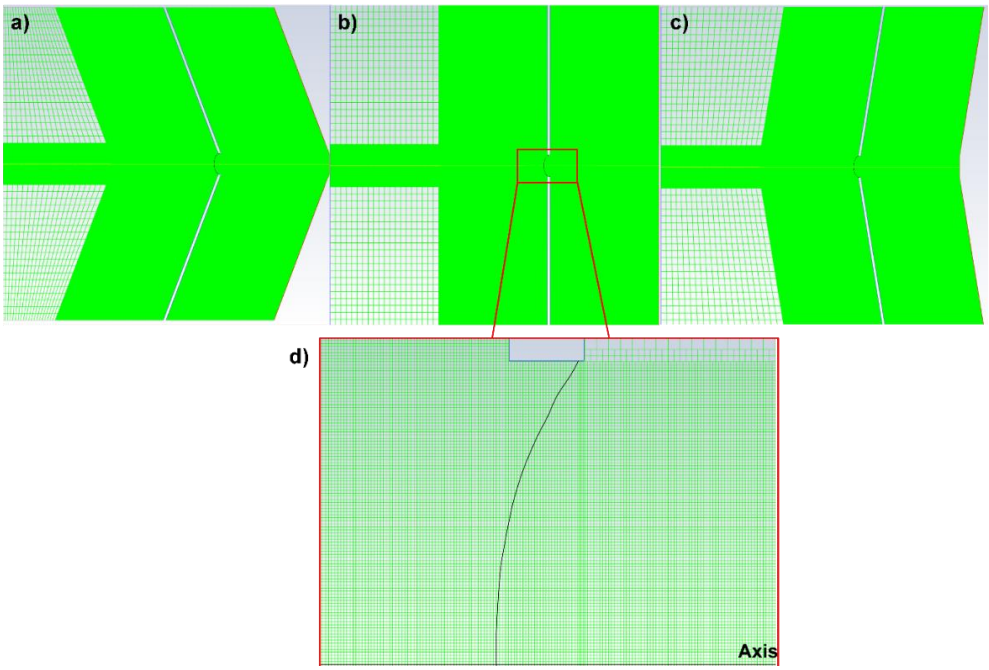

FIG. 4. Computational domains for angles (a) -20°, (b) 0°, and (c) 20° and d) a zoomed in image of the mesh closest to the nozzle.

The liquid used within the numerical simulations was silicon oil with a density of 936 kg/m^3 and a viscosity of 0.0087 kg/m-s. The surface tension coefficient was set to be 0.0231 N/m. For the boundary conditions, a velocity function at the inlet and 0 Pa gauge pressure at the outlet were set. The inlet velocity function was set to mimic the piston movement in order to provide the pressure pulse that creates and collapses the cavity. The velocity function and the corresponding pressure pulse are illustrated in Fig. 5 with the waveform characteristic parameters; velocity amplitude (v^-) and pulse width (t_p). For all the simulations, the pulse width was kept at 4 ms.

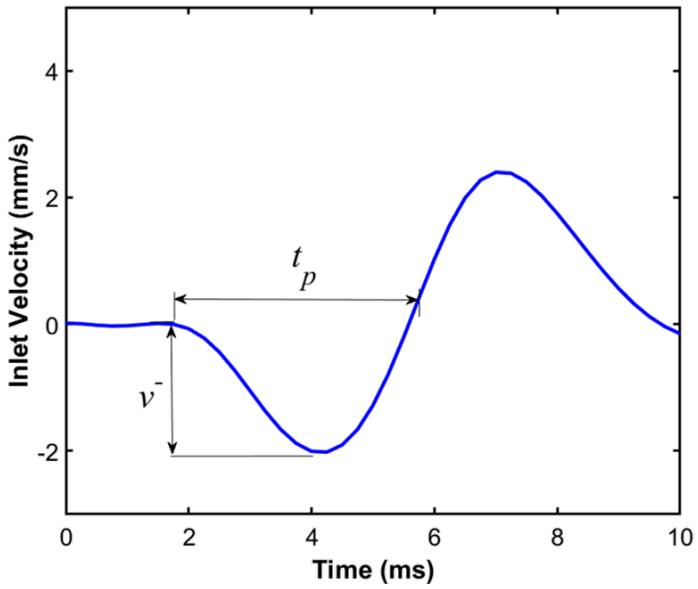

FIG. 5. Transient inlet velocity function.

Regarding the numerical methods, Pressure-Velocity Coupling scheme was set to PISO (Pressure-Implicit with Splitting of Operators) with a neighbour correction of one, which best suits transient flows with a small time-step because it reduces the number of iterations needed to be converged[18]. The selection for the Spatial Discretization gradient was Green-Gauss Cell based with the pressure correction following the Body Forced Weighted scheme. This was selected as it performs better in the problems where the densities change rapidly, which is the case across the interface. Momentum was solved using Third Order MUSCL (Monotone Upstream-Centered Schemes for Conservation Laws) as it improves spatial accuracy for structured mesh as it reduces the numerical diffusion[19]. Lastly, the volume fraction was tackled via the Geo-Reconstruct algorithm[20], as this is the most accurate algorithm to tackle simulations with a time-dependant solutions within the software. The Transient Formulation was set to First Order Implicit because it shows better stability and convergence of results with variable time step size, giving that we are using a Non-Iterative Time Advancement. The adaptive time advancement was selected with an initial time step of 1e-12s and maximum time step size of 0.0001s; the minimum and maximum step change factors were 0.5 and 5, respectively.

3. Results and Discussions

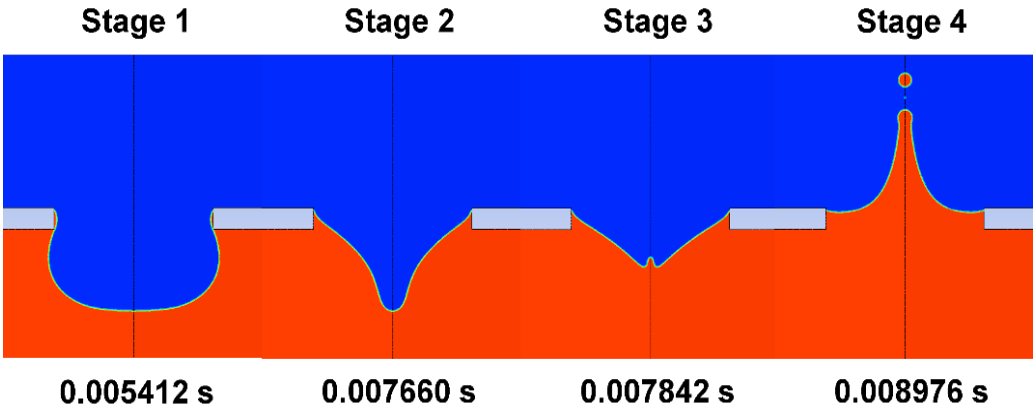

FIG. 6. Simulation of the different stages of cavity collapse at 0° with a Pulse Amplitude of 0.0023

The basis of the simulations conducted were to conclude whether variations in the nozzle angle, vessel height and vessel radius would cause the droplet diameter and subsequently, it's velocity to change. Simulations were conducted with the nozzle plate angle within the range of 20° to -20° ; the height of the fluid vessel was between 30mm to 2mm and the fluid vessel radius was set to be between 8mm to 20mm. As previously mentioned, a nozzle radius of 1mm was selected with the current working fluid being silicon oil and when one of the geometrical parameters was required to be changed, the others were set at their default values shown in Fig. 1. Previous works of research[17,21] concluded that there was an existing range of pulse amplitudes applied to the fluid that would result in a "Single Droplet Region", whereby only a single droplet would be ejected from the nozzle jet. It was shown that the values of pulse amplitude outside the observed ranges would either result in no droplet production (below the range) or multiple droplet production (above the range). The results shown in this work are only focusing on the single droplet region.

Before discussing the effects of changing the geometrical parameters, and how this might influence the size and velocity of the produced droplet, we need first to understand the full motion of a cavity collapse. The cycle of the droplet's generation out of a cavity collapse can be condensed into four main stages shown in Fig. 6. Stage 1 is the initial creation of the cavity, which is caused by the application of a negative pressure pulse (suction) inside the reservoir. Stage 2 is the rapid collapse of the cavity due to a subsequent positive pressure pulse (compression). This rapid collapse leads to stage 3, in which a jet much smaller than the nozzle size is nucleated at the centre. Eventually, at stage 4, the jet breaks into droplet/droplets through an end pinching mechanism. A contraction leading to pinching occurs at the tip of the jet (see Fig. 7) once there is enough kinetic energy to overcome the surface tension force. If the strength of the pulse is not great enough then there might be a collapse, but no droplet ejection. In this work, we used $\bar{v}$ to characterize the pulse strength provided to system.

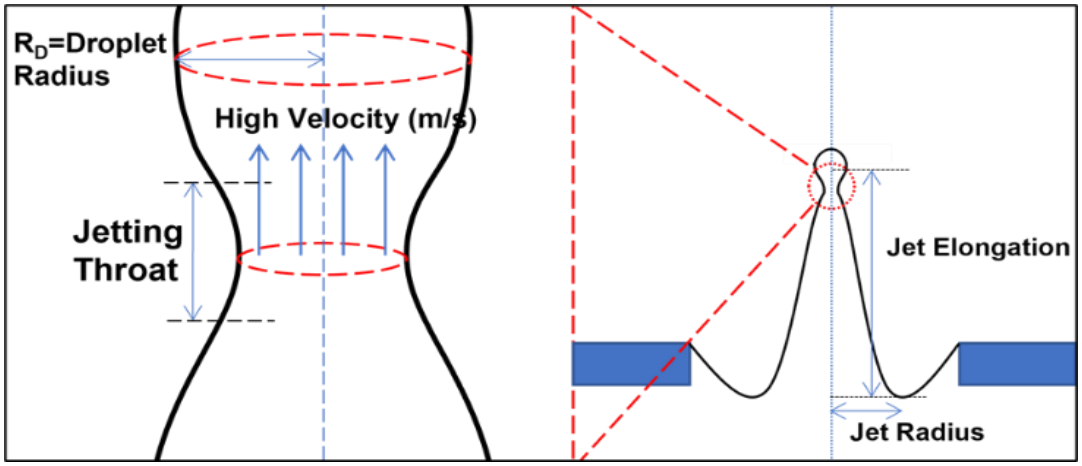

FIG. 7. Diagram of the moment before droplet detachment.

3.1 Height Variation of the Fluid Vessel

As mentioned previously, the value of *H* was examined from 2mm to 30mm. The droplet sizes produced for this range of vessel heights are depicted in Fig. 8. It is clear that changing the vessel height has an effect on the droplet size; decreasing the height leads to smaller droplets. However, this is not true for the entire examined range of height.

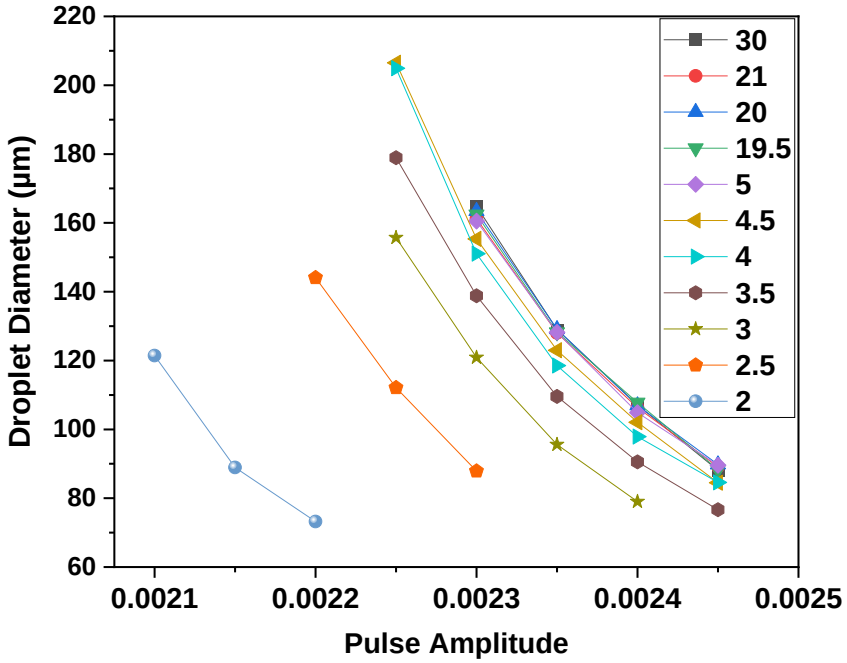

FIG. 8. Range of droplet sizes produced at different vessel height from 2 to 30mm, with varying Pulse Amplitudes.

This is obvious in Fig. 9, where you can see that the size of the ejected droplet is not affected by changing the vessel height as long as this height is much bigger than the nozzle size or the maximum cavity size. When the height becomes comparable to nozzle size, the wall effect on the cavity collapse starts to appear. This happens for height lower than 5 mm (H/R_0 = 5) regardless of the pulse amplitude. Below this threshold limit, the droplet size decreases by decreasing the vessel height.

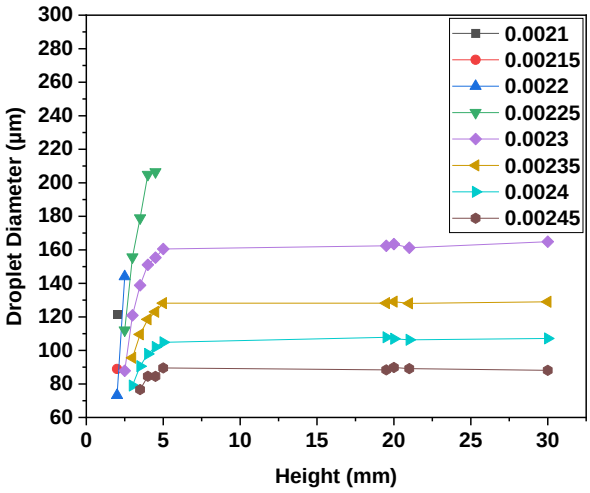

FIG. 9. Graphical representation of the variation in droplet diameter with varying vessel heights at different pulse amplitudes.

Changing the vessel height not only affects the droplet size when $H < 5R_0$ but also influences the droplet velocity. Fig. 10 shows that decreasing the height leads to a higher axial jet velocity and hence a faster droplet separated from the jet. These results are compatible with the scaling presented in previous work[9], which suggests an inverse relationship between the size of the droplet and the axial velocity of the jet produced out of a cavity collapse. Having the vessel height comparable to the cavity size means that the actuating piston (the inlet boundary in the simulation), that provides the pressure pulse to the system, is very close to the cavity created, which makes the collapse more aggressive.

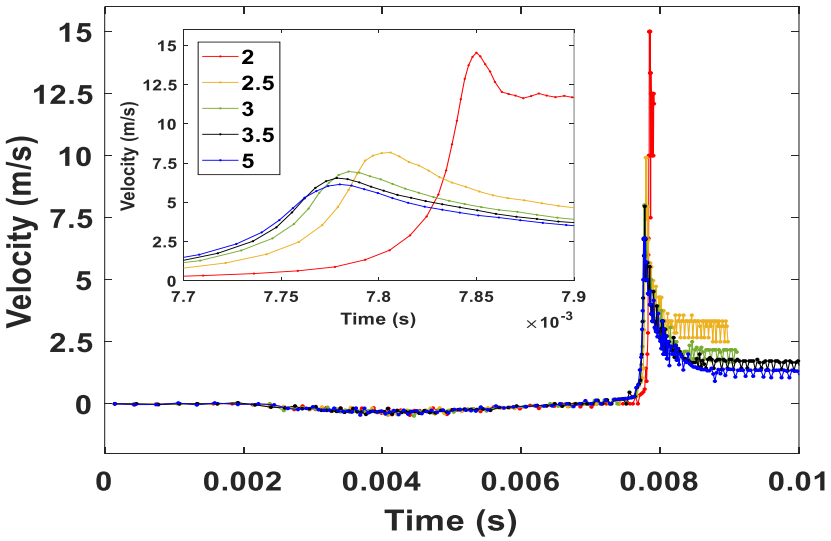

FIG. 10. A graph showing the velocity variation of the interface at the axis from cavity creation until droplet detachment, for vessel heights 2 to 5mm. The pulse amplitude is set at 0.0023. The subgraph is a zoom in to the velocity variation around the peaks.

This is evident in Fig. 11, which shows the pressure and radial velocity contours around the deformed cavity base. The maximum pressure and radial velocity are higher for smaller vessel height. We can see in Fig. 11, that the squeezing pressure and the radial velocity around the cavity base at H = 2.5 mm is higher than that at H = 5 mm which results in a thinner jet and subsequently a smaller droplet. The maximum pressure at the jet base is 7910 Pa for H =2.5 mm and 6320 Pa for H =5 mm. This also explains why, at smaller vessel height, the produced jet and subsequently the separated droplet would have a higher velocity.

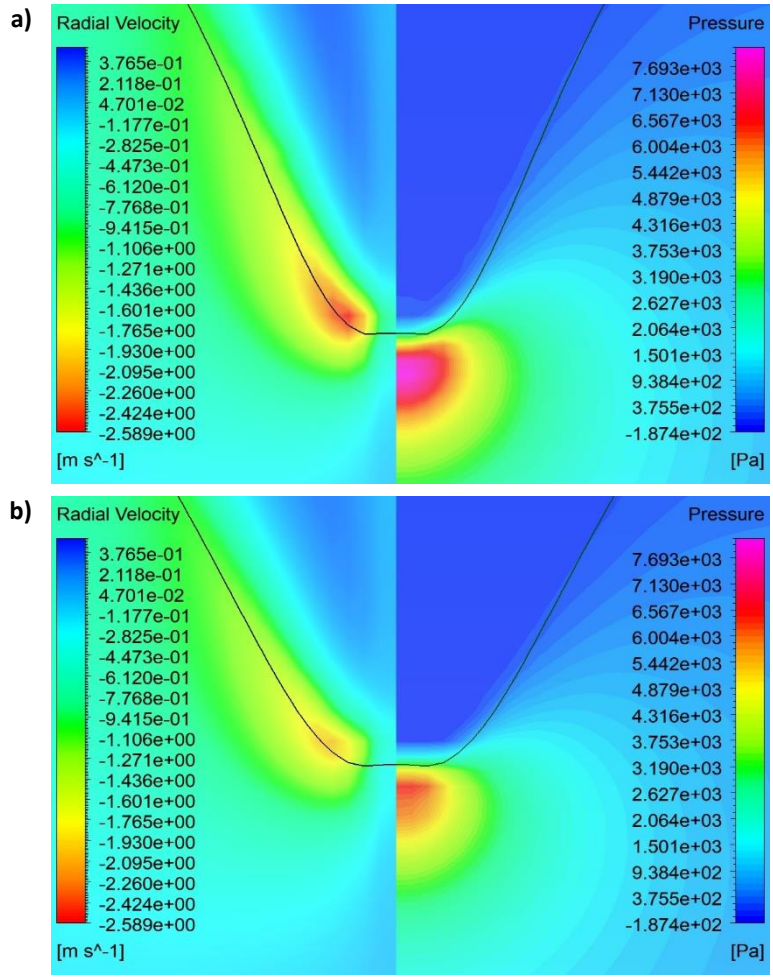

FIG. 11 Velocity and pressure contours at pulse amplitude of 0.0023 for vessel height of a) 2.5mm and b) 5mm with the original radius of 15mm.

3.2 Radius Variation of the Fluid Vessel

For the range of fluid vessel radius examined, 8mm≤ R ≤ 20mm, it was found that as the vessel radius increased, the value of the droplet diameter decreased as graphically shown in Fig. 12.

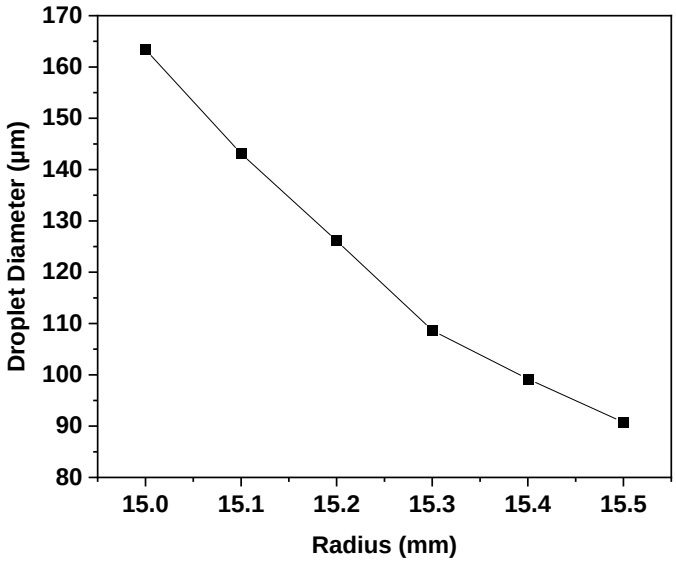

FIG. 12. Variation in droplet diameter when the vessels' radius is changed. This data is collected at a pulse amplitude of 0.0023.

It was also noticed that decreasing the vessel radius shifts the range of pulse amplitude required to produce a single droplet. The data graphically plotted in Fig. 13 shows that decreasing a vessel radius from 20 to 10mm, would require 5 times the increase in pulse amplitude to produce the same droplet size. This shift in the pulse amplitude does not considerably change the range of droplet sizes that can be generated within the single droplet region.

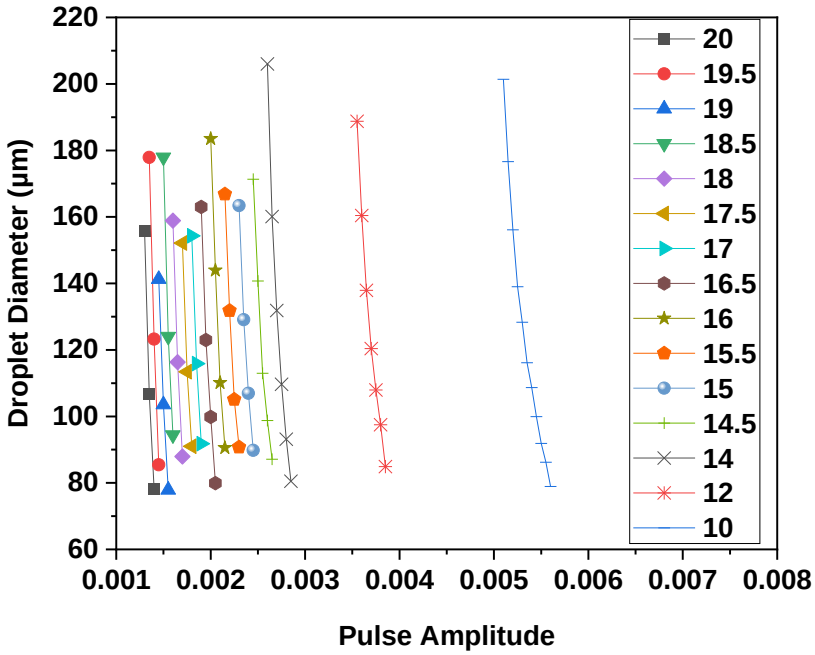

FIG. 13. Droplet diameter versus pulse amplitude for vessel radius from 10 to 20mm with varying Pulse Amplitudes.

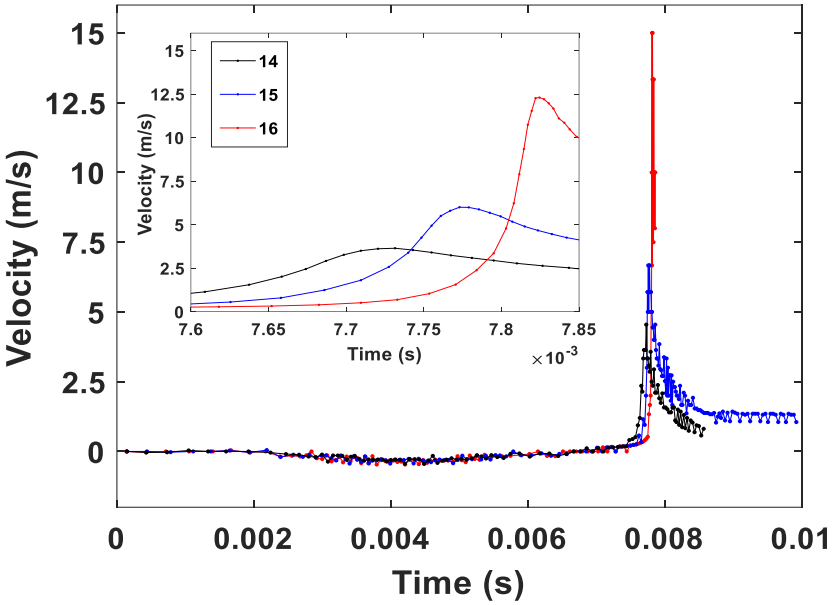

FIG. 14. A velocity profile graph showing the variation of velocity, vessel radius 14, 15.5, and 16 mm. The velocity is taken along the fluid interface and the pulse amplitude is set at 0.002. The subgraph is a zoom in to the velocity variation around the peaks.

The data presented in Fig. 12 shows that a gradual change in the vessel radius, in increments of 0.1mm, results in a significant effect on the droplet diameter; an increase of 0.5mm caused the droplet size to decrease from 163.399 μm to 90.7389 μm, even when the vessel radius is much bigger than the nozzle radius. As expected, the axial jet velocity is also influenced by the vessel radius; increasing the vessel radius leads to higher axial jet velocity profile (see Fig. 14) and subsequently, a faster droplet. This result might be surprising as one might expect that there is no wall effect on the cavity collapse when $R>>R_0$, hence the size and velocity of the produced droplet should not be changing with the vessel radius.

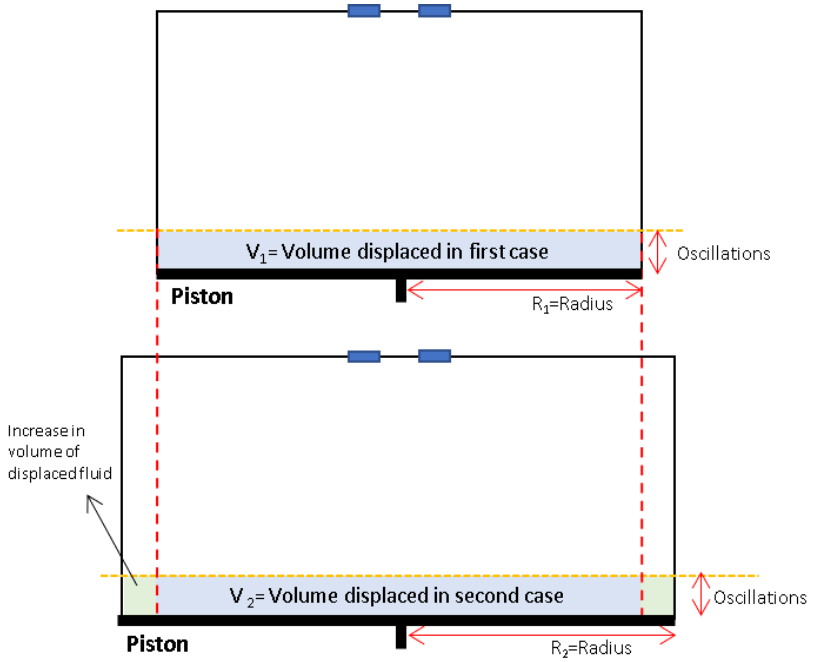

FIG. 15. A diagram illustrating the increase in the volume of fluid displaced due to an increase in radius size.

To explain the reason behind this, we need to recall the physical cavity collapse device that we are replicating within our simulation. When the vessel radius is increased from R_1 to R_2, as shown in Fig. 15, the volume of liquid being displaced by the downwards motion of the piston is increased from V_1 to V_2, with the addition of the extra fluid shown on the sides. This displacement of liquid has a direct correlation with the size of the maximum volume of cavity created before the collapse; a larger volume of fluid displaced at the base of the vessel means a larger cavity created at the nozzle. To confirm this, we compared the cavity interface at vessel radius 14mm and 16mm at the same pulse amplitude. Fig. 16 (a) shows clearly that increasing the vessel radius led to an increase in the cavity volume. The excess volume of displaced liquid, when the vessel radius was changed from 14mm to 16mm with the corresponding difference in maximum cavity volume, was measured, and it was verified that they both had the same value of 0.716 mm^3. Our simulation reveals that this increase in the cavity size leads to smaller and faster droplets. This is because, for a larger cavity, the interface curvature is longer as indicated in Fig. 16 (a), which allows for more expansion in the axial direction downwards (see Fig. 16 (b)). This would create a smaller cavity base and thus allowing the nucleation of a smaller jet, and subsequently a smaller droplet (see Fig. 16 (c)).

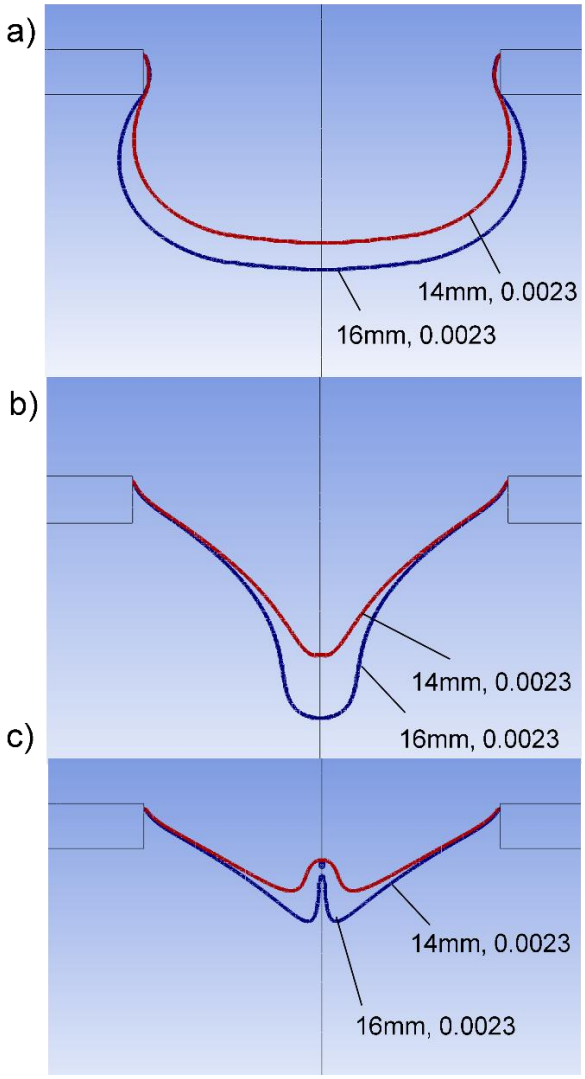

FIG. 16. (a) The difference in the maximum created cavity for vessels with radius 14 and 16mm, at a pulse amplitude of 0.0023. (b) Shows the extra elongation for the bigger cavity. (c) Shows the difference in jetting size caused by the difference in cavity volume for 14 and 16mm vessel radius.

Considering the inverse relation between the jet velocity and the drop size, increasing the cavity size should then increase the axial jet velocity. These results are actually contradictory to what have been mentioned in previous works[6,12,22]. It was reported that decreasing the size of the collapsed bubble favours the damping of capillary waves, which weaken the jet velocity. Hence, a smaller cavity leads to an increase in the jet velocity. Perhaps the reasoning behind this discrepancy between our results and the literature is the difference in configuration between the collapse of a cavity created at a nozzle and a bubble at a free surface. In the latter case, because the cavity interface is not pinned to a nozzle at the rim, it keeps expanding in the radial direction, which halts the formation of smaller cavity base and therefore, leads to a bigger and slower ejected jet.

3.3 Angle Variation of the Ejecting Nozzle

Within this report, we evaluated the effect of the plate nozzle angles by examining angles 20°, 10°, 0°, -10°, and -20°. Fig. 17 shows how the angle of the nozzle plate alters the droplet size produced out of the cavity collapse. Increasing the angle in the positive direction, with the same pulse amplitude, leads to smaller droplet. On the other hand, increasing the angle in the negative direction, results in a bigger droplet. The angle of the nozzle plate influences not only the droplet size, but also the range of pulse amplitudes and droplet sizes in which only a single droplet can be produced; changing the angle from 20° to -20° would increase the range of droplet sizes that can be produced. Fig. 17 also shows clearly the maximum and minimum bounds for the single droplet region. At both these bounds, the droplet size increases from 20° to -20°, with rate at the maximum bound higher than that of the minimum bound.

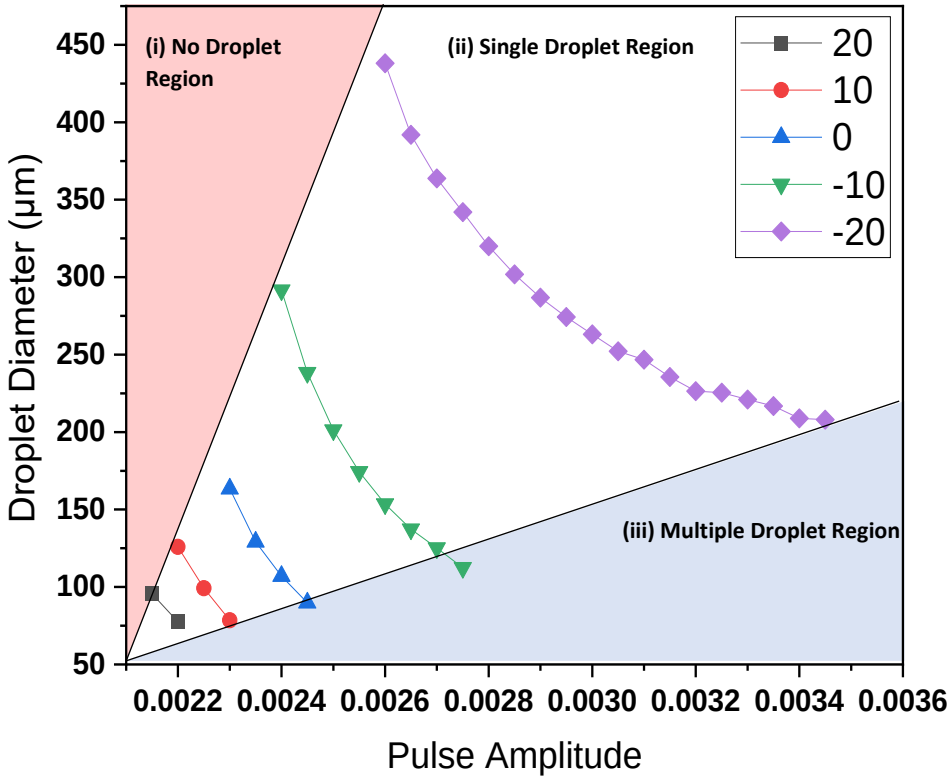

FIG. 17. Graphical representation of how the droplet diameter varies with pulse amplitude for different nozzle angles.

The simulation indicates that the first stage of cavity collapse is kept consistent regardless of the angle change (see Fig. 18a); however, variation starts to happen at the very end of this stage,

when the cavity base becomes comparable in size to the ejected jet. The effect of the plate nozzle angle is clear in Fig. 18b. The cavity base, just before the jet nucleation, gets smaller from -20° to 20°, which results in smaller generated jet and subsequently smaller droplet as it can be seen in Fig. 18c.

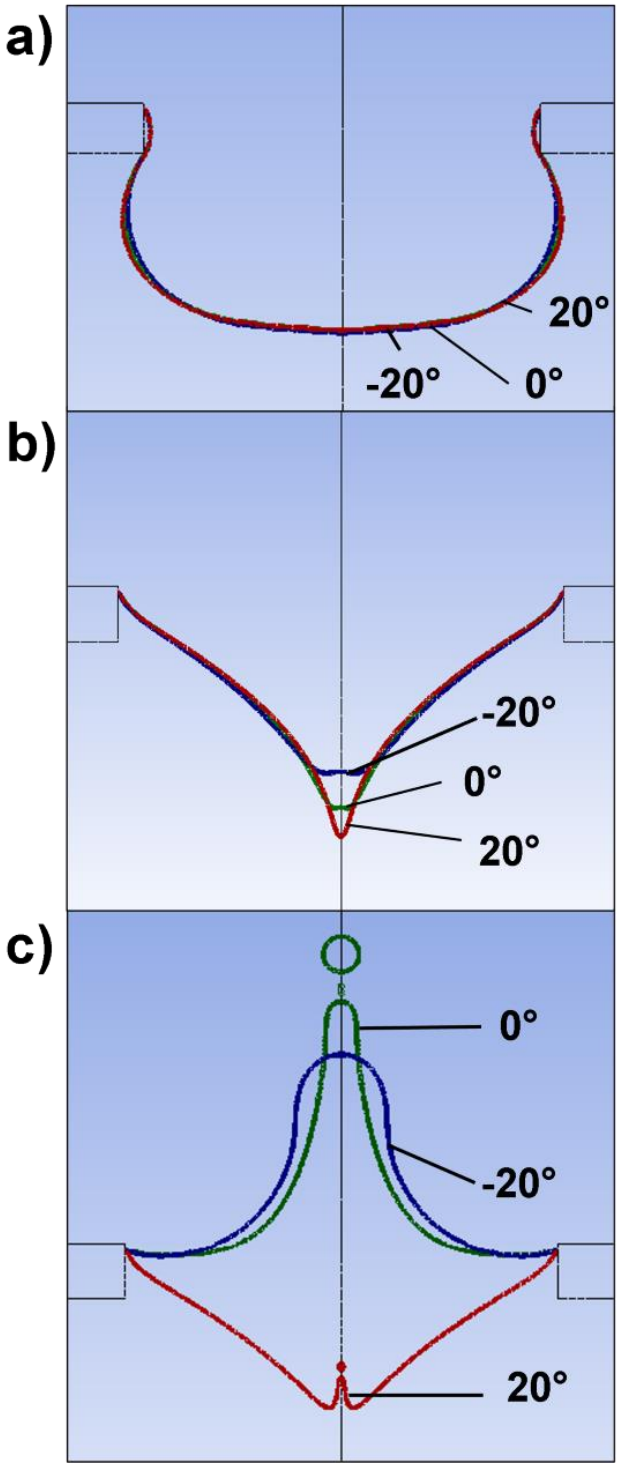

FIG. 18. Cavity collapse jetting for nozzle angles -20°, 0°, and 20° at stages (a) cavity creation (b) cavity squeezing and (c) jetting (with the inclusion of satellite droplets). Simulations were conducted at pulse amplitude of 0.0023. It is to be noted that images a) and b) are taken at the same time value for all three angles, whereas image c) consists of all three angles at different time values. At Angle 20°, the image is taken at 0.00781877s, at Angle 0° is taken at 0.00890048s and at Angle -20° is taken at 0.00918406s. Angles 0° and 20° are taken at the drop pinching moment.

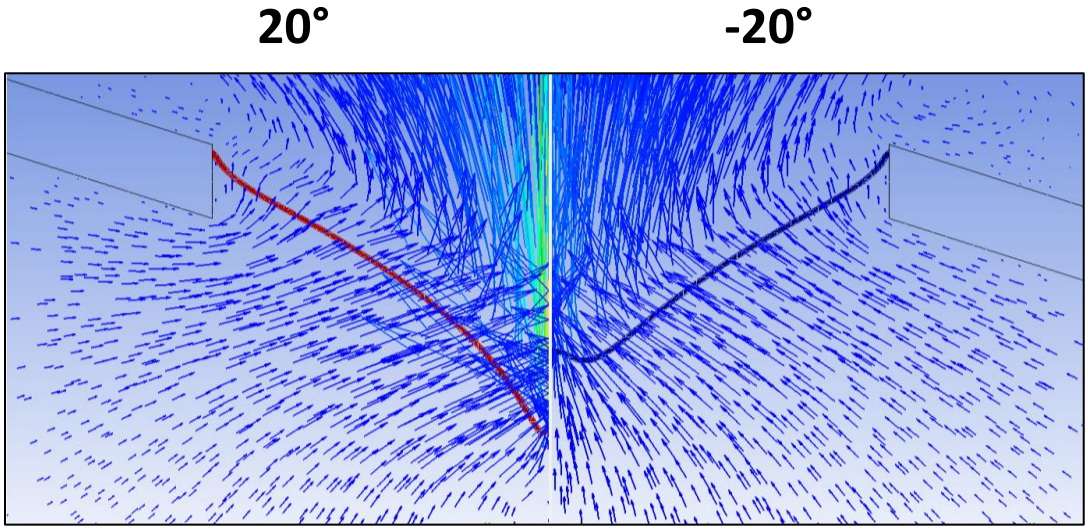

FIG. 19 Difference in velocity vectors between -20° and 20° at a pulse amplitude of 0.0023.

The reason behind this effect is that changing the angle from -20° to 20° allows for more expansion of the cavity base along the axis, and hence helps to reduce the cavity base size at the moment of jet nucleation, leading to a smaller jet. This extra expansion of the cavity base is directly related to the direction of the velocity vectors, which is affected by the nozzle plate angle. Fig. 19 shows the difference in velocity vectors between the nozzle plate angles 20° and -20°, just before the jet nucleation. The flow direction seems to change the cavity curvature from -20° to 20° allowing for more squeezing and expansion to the cavity base in the latter case. The effect of the flow direction is evident in Fig. 20(a), which shows the radial velocity contours for two nozzle plate angles. The radial velocity acting on the cavity base sides in 20° is clearly higher than in -20° which results in smaller base and hence nucleation of smaller jet. At the same time, the axial velocity acting on the cavity base is higher for the 20° nozzle angle (see Fig. 20(b)) leading to faster nucleated jet.

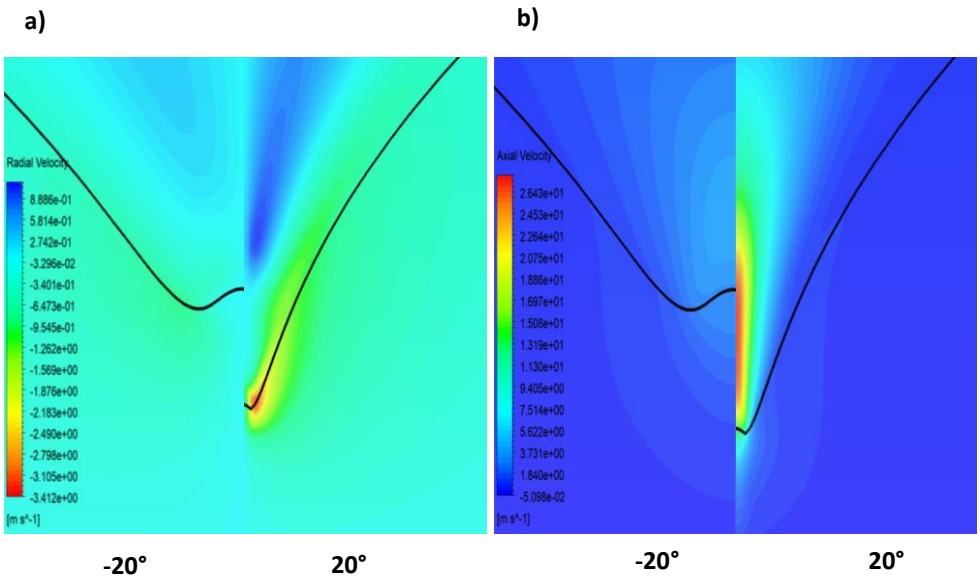

FIG. 20. Comparison between nozzle angles -20º and 20º, at cavity squeezing stage, showing (a) the radial velocity contours and (b) the axial velocity contours. Simulations were done at a pulse amplitude of 0.0023.

4. Conclusion

In this report, it has been discussed and explained how varying the ejecting nozzle angle, height, and radius of the fluid vessel, in a controlled cavity collapse device, has caused a change to the top jet drop. Several means of data were compiled and compared with each other to conclude the following. The droplet size is directly proportional to the height of the fluid vessel, but only when $H/R_0 < 5$. For vessel heights higher than this threshold limit, there is no change to the droplet size. On the other hand, the droplet size decreases when the radius of the fluid vessel is increased. This happens even if $R >> R_0$, mainly because the extra displaced liquid, due to the increase in vessel radius, leads to an increase in the volume of the cavity created. Therefore, the cavity interface expands further along the axis during the compression stage, allowing for a more squeezed cavity base and hence a smaller generated jet and droplet. Lastly, as the nozzle plate angle is varied in the positive direction, the size of the produced droplet decreases and the velocity increases. Rotating the angle in the negative direction, would lead to an increase in the droplet size and subsequently a decrease in drop velocity. It was established that the nozzle plate angle has an effect on the top jet droplet due to the change in the direction of the flow acting on the cavity base. The radial velocity component of the velocity vectors increases for a higher nozzle plate angle, leading to more squeezing and expansion of the cavity base. This leads to a thinner jet and subsequently a smaller and faster generated droplet.

ACKNOWLEDGMENTS

This work was supported by the Engineering and Physical Sciences Research Council (United Kingdom) under Grant No. EP/V04382X/1.

AUTHOR DECLARATIONS

Conflict of Interest

The authors report no conflict of interest.

DATA AVAILABILITY

The data that support the findings of this study are available from the corresponding author upon reasonable request

REFERENCES

[1] Nuyttens, D., De Schampheleire, M., Verboven, P., Brusselman, E. and Dekeyser, D., 2009. Droplet size and velocity characteristics of agricultural sprays. Transactions of the ASABE, 52(5), pp.1471-1480

[2] Lemmo, A. V., J. T. Fisher, H. M. Geysen, and D. J. Rose, 1997. Characterization of an Inkjet Chemical Microdispenser for Combinatorial Library Synthesis. Anal. Chem. 69, 543.

[3] Basaran, O.A., 2002. Small-scale free surface flows with breakup: Drop formation and emerging applications. AIChE Journal, 48(9), pp.1842-1848. Annu. Rev. Fluid Mech. 47, 507.

[4] Morey, M., Fernández-Marmiesse, A., Castineiras, D., Fraga, J.M., Couce, M.L. and Cocho, J.A., 2013. A glimpse into past, present, and future DNA sequencing. Molecular genetics and metabolism, 110(1-2), pp.3-24.

[5] Jiang, X., Rotily, L., Villermaux, E., and Wang, X., 2022. Submicron drops from flapping bursting bubbles, Proc. Natl. Acad. Sci. U.S.A., 119, e2112924 119.

[6] Deike, L., Ghabache, E., Liger-Belair, G., Das, A. K., Zaleski, S., Popinet, S., and Séon, T., 2018. Dynamics of jets produced by bursting bubbles, Phys. Rev. Fluids, 3, 013 603.

[7] Bourouiba, L., 2021. The fluid dynamics of disease transmission. Annu. Rev. Fluid Mech. 53, 473–508.

[8] Sampath, K., Afshar-Mohajer, N., Chandrala, L.D., Heo, W.-S., Gilbert, J., Austin, D., Koehler, K. & Katz, J., 2019. Aerosolization of crude oil-dispersant slicks due to bubble bursting. J. Geophys. Res. 124 (10), 5555–5578.

[9] F. Veron., 2015. Ocean spray. Annu. Rev. Fluid Mech. 47, 507.

[10] Brooks, S. D. and Thornton, D. C. O., 2018. Marine Aerosols and Clouds, Annu. Rev. Marine Sci., 10, 289–313.

[11] Bertram, T. H., Cochran, R. E., Grassian, V. H., and Stone, E. A., 2018. Sea spray aerosol chemical composition: Elemental and molecular mimics for laboratory studies of heterogeneous and multiphase reactions, Chem. Soc. Rev., 47, 2374–2400.

[12] J. B. Keller, A. King, and L. Ting, 1995. Blob Formation, Phys. Fluids 7, 226

[13] S. Krishnan, E. J. Hopfinger, and B. A. Puthenveettil, 2017. On the scaling of jetting from bubble collapse at a liquid surface, J. Fluid Mech. 822, 791.

[14] E. Ghabache and T. Séon, 2016. Size of the top jet drop produced by bubble bursting, Phys. Rev. Fluids 1, 051901.

[15] A. M. Gañán-Calvo, 2017. Revision of Bubble Bursting: Universal Scaling Laws of Top Jet Drop Size and Speed, Phys. Rev. Lett. 119, 204502.

[16] Castrejón-Pita, A.A., Castrejón-Pita, J.R. and Martin, G.D., 2012. A novel method to produce small droplets from large nozzles. Review of scientific instruments, 83(11), p.115105.

[17] Said Ismail, A., Gañán-Calvo, A.M., Castrejón Pita, J.R., Herrada Gutiérrez, M.Á. and Castrejón Pita, A.A., 2018. Controlled cavity collapse: scaling laws of drop formation. Soft Matter, 14, 7671-7679.

[18] R.I Issa, A.D Gosman, A.P Watkins, 1986. The computation of compressible and incompressible recirculating flows by a non-iterative implicit scheme. Journal of Computational Physics, 62, 66-82.

[19] B. Van Leer, 1979. Toward the Ultimate Conservative Difference Scheme. IV. A Second Order Sequel to Godunov's Method. Journal of Computational Physics. 32, 101–136.

[20] D. L. Youngs, 1982. Time-Dependent Multi-Material Flow with Large Fluid Distortion, Numerical Methods for Fluid Dynamics. Academic Press: Cambridge, MA, USA.

[21] Fromm, J.E., 1984. Numerical calculation of the fluid dynamics of drop-on-demand jets. IBM Journal of Research and Development, 28(3), pp.322-333.

[22] L. Duchemin, S. Popinet, C. Josserand, and S. Zaleski, 2002. Jet formation in bubbles bursting at a free surface, Phys. Fluids 14, 3000.